Electronic polarons and bipolarons in iron-based superconductors: The role of anions

Mona Berciu, Ilya Elfimov, and George A. Sawatzky
Department of Physics and Astronomy, University of British Columbia, Vancouver, British Columbia, Canada V6T 1Z1
(Received 28 March 2009; revised manuscript received 14 May 2009; published 5 June 2009)

We introduce a quantum-mechanical model to describe the low-energy scale electronic structure of the Fe-based pnictides, placing a special importance on the large polarizability of the large anions, such as As^{3-}. These are modeled in terms of an atomic two-level system coupled strongly to charge fluctuations on the nearby Fe ions. This strong coupling results in electronic polaron formation, a strong effective reduction in the Fe on-site Coulomb repulsion, and the appearance of a strong attractive interaction for d electrons on nearest-neighbor Fe sites, which could be an essential component of the pairing mechanism. This quantum model allows us to investigate this phenomenology away from the linear regime and to also study the dynamic properties of these polarons, as well as the binding of polaron pairs and their dynamics.

DOI: 10.1103/PhysRevB.79.214507 PACS number(s): 74.20.Mn, 74.70.−b

I. INTRODUCTION

Superconductivity is a fascinating example of how "more is different."[1] It is due to electrons binding into bosonic Cooper pairs, which exhibit coherent behavior across a macroscopic sample. Finding the mechanism responsible for this binding is one of the more difficult tasks of condensed-matter physics. For conventional superconductors the solution was given by the BCS theory[2] as being due to exchange of phonons. For the cuprate high-T_c superconductors[3] a widely accepted pairing mechanism is still missing, despite intense effort. The recently discovered Fe-based high-T_c superconductors present us now with a new challenge.[4–8]

At first sight, one may expect the behavior of pnictides to be related to that of the cuprates, given the somewhat similar layered structures. However, there is an essential difference between the CuO_2 layer where the important physics takes place in a cuprate, and its counterpart, the FeAs layer of a pnictide: while the former is two dimensional (2D), with all Cu and O atoms in the same layer, the latter is not. Instead, the layer hosting the Fe atoms (which are arranged on a simple square lattice) is sandwiched between two layers which share equally the As atoms, as sketched in Fig. 1. Each Fe has four nearest-neighbor (nn) As atoms at a distance $R=2.4$ Å, arranged in a somewhat distorted tetrahedron, two in the upper and two in the lower layer.

The different geometry has important consequences. In the cuprates, the states near the Fermi energy E_F consist of strongly hybridized Cu $3d$ and O $2p$ orbitals. In contrast, hardly any hybridization appears between the Fe $3d$ and As $4p$ orbitals within 1–2 eV of the Fermi energy, with the former giving essentially all the contribution to the low-energy states of the pnictide.[9] This lack of hybridization is due not only to the lattice geometry but also to the substantial spread in space of the As $4p$ orbitals, as compared to the O $2p$ orbitals.

As a result, one might assume that the simplest Hamiltonian describing the low-energy physics of pnictides is a Hubbard Hamiltonian for the Fe $3d$ electrons, namely,

$$\mathcal{H}_{\mathrm{Fe}} = -\sum_{i,j,\sigma} (t_{ij} c^{\dagger}_{i,\sigma} c_{j,\sigma} + \mathrm{h.c.}) + U_H \sum_i \hat{n}_{i\uparrow}\hat{n}_{i\downarrow}, \qquad (1)$$

where $c^{\dagger}_{i,\sigma}$ creates an electron on the Fe site i with spin σ and $\hat{n}_{i\sigma}=c^{\dagger}_{i\sigma}c_{i\sigma}$. For simplicity, in this work we use a single-band model where we only count "doping" electrons, i.e., charges on top of the $3d^6$ configuration of the Fe in the undoped compound. In reality a multiple-band Hamiltonian should be used for the proper description of the various $3d$ orbitals; however the essential physics we want to discuss is already captured within this simpler starting point. The hopping to As sites is neglected because of the small hybridization near E_F.

Hamiltonian (1) is, of course, the most common starting point for describing cuprate physics. There it does include the contribution of O anions because in that context $c^{\dagger}_{i,\sigma}$ are operators for Zhang-Rice singlets.[10] In contrast, using Eq. (1) or a similar starting point either in the strong-coupling[11–16] or weak-coupling limit[17–20] as the low-energy Hamiltonian for pnictides implies that the As anions play no role in their physics.

However, the As anions are highly polarizable, big ions which are strongly influenced by the presence of extra charges in their vicinity. As pointed out in Ref. 9, one expects each doping charge to be surrounded by polarized As ions, giving rise to *electronic polarons*. This results in a strong screening of the on-site Coulomb repulsion, suggesting that these materials are not in the large U limit of a Mott-Hubbard insulator. It also results in a strong nn attraction, which is certainly a (if not the) key component in the pairing mechanism. The arguments of Ref. 9 are based on semiclassical estimates.

In this paper we introduce a quantum-mechanical model to describe the low-energy scale electronic structure of the Fe pnictides, based on the physics described in Ref. 9. This model places special importance on the large polarizability of the large anions, such as As^{3-}, which we model in terms

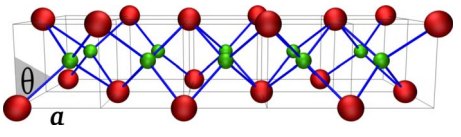

FIG. 1. (Color online) Three-dimensional sketch of the FeAs layer. The small (green) spheres indicate Fe and the large (red) ones indicate As locations. The lattice constant is a and the angle θ between the Fe-As direction and the z-axis is indicated.

of an atomic two-level system coupled strongly to charge fluctuations on the nearby Fe ions. Like in the semiclassical model of Ref. 9, this strong coupling results in electronic polaron formation, a strong effective reduction in the Fe on-site Coulomb repulsion, and the appearance of a strong nearest-neighbor attractive interaction for d electrons on Fe sites. The quantum model allows us to investigate this phenomenology away from the linear regime and to also study the dynamic properties of these polarons, as well as the binding of polaron pairs and their dynamics.

Our model has similarities with the lattice polaron,[21] the Little,[22] and the Allender, Bray, and Bardeen[23] (ABB) excitonic models for superconductivity; however there are also essential differences which circumvent the main objections raised concerning them. As demonstrated below, our model results in rather modest mass enhancements for the electronic polaron and, most importantly, leads to an attractive term in the *nearest-neighbor* interactions, strongly reducing the need for huge retardation effects required to overscreen the on-site repulsion in all these other models. In addition, we demonstrate that the bipolaron masses—if they do form bound states—are rather modest, being only three to four times the mass of a single polaron. This, again, is very different from the lattice polaron or the Little or ABB on-site pairing models. Our model also has superficial similarities with the theory of hole superconductivity proposed by Hirsch and co-workers;[24–26] however they are based on very different scenarios. While we believe that the pairing charge carriers are hosted in Fe $3d$ orbitals and the anions' role is encompassed through their polarizability, in their scenario the anions are hosting the pairing holes and their polarizability is irrelevant.[27] Moreover, their pairing mechanism is essentially the same in pnictides as in cuprates.[26] As discussed in detail below, in our model the specific off-plane location of the anions is essential in giving rise to the large effective nn attraction. The same mechanism applied to a CuO_2-like planar structure gives rise to strong nn repulsions, instead of pairing.

The article is organized as follows: in Sec. II we introduce our model and parameters. In Sec. III we analyze properties of a single electronic polaron, while in Sec. IV we discuss properties of bound bipolarons. Section V contains our summary and discussions.

II. MODEL

The idealized FeAs layer of interest is sketched in Fig. 1, which shows the cubic lattice (lattice constant $a=2.8$ Å) which has the Fe in the center of the cubes, on a simple square lattice. The real structure has somewhat distorted tetrahedra, and can be described by a simple generalization of our idealized model.

As discussed, we assume that the valence electrons occupy $3d$ orbitals of the Fe atoms. We are interested in the excess charges on the Fe sites and describe them in an effective single-band model, like in Eq. (1). We assume that they can hop between nearest-neighbor Fe atoms, with a hopping integral t, and also consider separately the effect of second-nearest-neighbor hopping, with a hopping integral t'. There is very little hybridization of these $3d$ orbitals with As $4p$ or $5s$ orbitals near the Fermi energy, and we ignore it altogether.[9] On-site Hubbard repulsion for these charges, characterized by an energy U_H, is also included. Thus, the hopping Hamiltonian for the extra charges on the Fe sites is taken to be

$$\begin{aligned}\mathcal{H}_{\mathrm{Fe}} &= \hat{T} + \hat{T}' + \hat{U} \\ &= -t \sum_{\langle i,j\rangle,\sigma} (c^{\dagger}_{i,\sigma} c_{j,\sigma} + \mathrm{h.c.}) - t' \sum_{\langle\langle i,j\rangle\rangle,\sigma} (c^{\dagger}_{i,\sigma} c_{j,\sigma} + \mathrm{h.c.}) \\ &\quad + U_H \sum_i \hat{n}_{i\uparrow} \hat{n}_{i\downarrow}, \end{aligned} \tag{2}$$

where $\langle i,j\rangle, \langle\langle i,j\rangle\rangle$ denote summation over nearest and second-nearest-neighbor Fe sites, respectively. A more detailed model taking in consideration all relevant $3d$ orbitals is of course possible, but not necessary for our purposes. We avoid this complication in order to make the physics uncovered in our model more transparent.

Ab initio calculations find that the anions are effectively in the As^{3-} state, with fully occupied $4p$ bands lying well below the Fermi energy.[9] In reality, these As $4p$ states are strongly hybridized with Fe $4s$ and $4p$ orbitals (this hybridization is responsible for the fact that the effective As charge inside the muffin tin is much less[9] than the ionic charge of -3). Since this mixing is strongly dependent on the Fe $3d$ occupation, it will provide a screening mechanism for the bare Coulomb repulsion, in particular for the value of U_H. In the following we consider that such screening is already included in U_H. For simplicity, we also refer only to the full As $4p$ orbitals, ignoring their hybridization with the Fe $4s$ and $4p$ orbitals (this could also be accounted for in a multiband model, but is of limited relevance and we ignore it for clarity).

In our model, the only role of these As anions is that they become polarized due to the electric field created when an extra charge is on a nearby Fe atom. This is due to transitions of As electrons from the filled $4p$ shell into (primarily) the empty $5s$ shell, and results into a dipole moment (polarization cloud) pointing toward the Fe atom which hosts the extra charge. For simplicity, we make two approximations regarding the interactions: (i) only the four As atoms closest to an Fe hosting a charge are polarized by its electric field, and (ii) we ignore dipole-dipole interactions between As clouds. The quantitative importance of these approximations is discussed below.

Three more observations are in order. First, it is more convenient to describe the As polarization clouds not in terms of an electron being excited from the filled $4p$ orbitals into the empty $5s$ orbital but, equivalently, in terms of a hole being excited from the $5s$ into the $4p$ orbitals. Thus, each As will be described by four operators: $s^{\dagger}_{\sigma}, p^{\dagger}_{x,\sigma}, p^{\dagger}_{y,\sigma}, p^{\dagger}_{z,\sigma}$, which create a hole of spin σ in the respective orbital. The ground state, then, is $s^{\dagger}_{\uparrow} s^{\dagger}_{\downarrow} |0\rangle$ and the p orbitals lie at an energy Ω above it. If we measure energies above the s orbital, the Hamiltonian of the unperturbed As ions is

$$\mathcal{H}_{\mathrm{As}} = \Omega \sum_{i,\lambda,\sigma} p^{\dagger}_{i,\lambda,\sigma} p_{i,\lambda,\sigma}, \tag{3}$$

where i runs over the locations of the As atoms (see Fig. 2 for site labeling convention), $\lambda = x, y, z$, and σ is the spin of the hole.

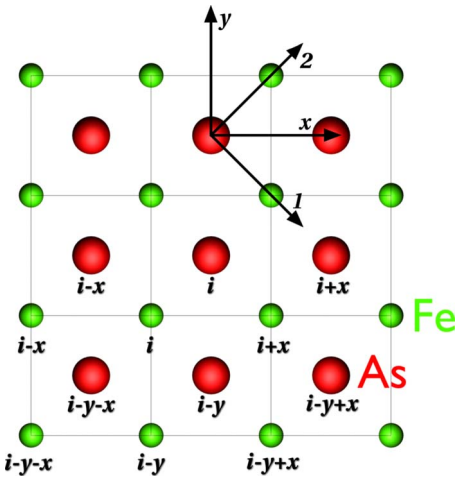

FIG. 2. (Color online) View from above of the Fe-As structure. Several sites are indexed. The orientations of the in-plane axes 1,2 and x,y is also indicated. The Fe and As layers have different depths in the z direction.

The second observation is that this Hamiltonian ignores hopping of charges between As atoms. This is a reasonable approximation given the large distance between neighbor As atoms, which results in rather narrow As bands, as demonstrated by *ab initio* calculations. Physically, we expect hopping of a single charge between As ions to be inhibited because of Coulomb on-site repulsion. Hopping of the excitonlike particle-hole pair describing the polarization cloud is not inhibited; however this is likely a heavy object, given the rather narrow As bands. As we demonstrate below, the electronic polarons and bipolarons of interest to us are very light and highly mobile objects. In comparison, we can assume the excitonlike polarization clouds to be infinitely heavy, i.e., not allowed to move between different As sites on the time scales of interest to us. This is why we model the As within this rather atomistic picture.

Finally, the lattice illustrated in Fig. 1 suggests that we should consider a unit cell with (a minimum of) two Fe and two As atoms, one in the top and one in the bottom layer. However, given our simplifications, in our model it makes no difference whether half the As are above and half are below the Fe layer, or whether they are all in the same plane (for example, in the layer below the plane of Fe). Mathematically, this follows because for the As in the layer above, one can redefine the p_z operators as $p_z \to -p_z$, which is equivalent to a local flipping of the direction of the z axis. This is very convenient because it allows us to use a simple unit cell with one Fe and one As in the basis, as illustrated schematically in Fig. 2. However, it is important to point out that if one wants to include, for example, As dipole-dipole interactions, then one needs to carefully consider the true orientations of the As polarization clouds with respect to one another.

Figure 2 also shows how we index the lattice sites, with Fe_i and As_i being the unit cell of the simple square lattice. If the charge is on Fe_i, the polarization of As_i and the other three As neighbors is pointing in its direction. It is therefore more convenient to use for the in-plane directions the 1,2 axes (see Fig. 2), and $3=z$ for the out-of-plane direction, in terms of which $p_1=\frac{1}{\sqrt{2}}(p_x-p_y)$, $p_2=\frac{1}{\sqrt{2}}(p_x+p_y)$, $p_3=p_z$, and $\mathcal{H}_{\mathrm{AS}}$ remain formally identical to that of Eq. (3), except that now $\lambda=1,2,3$.

With these definitions, the cloud of As_i is pointing toward Fe_i in the direction $\vec{e}=-\sin\theta\vec{e}_2+\cos\theta\vec{e}_3$, where $\cos\theta=\frac{1}{\sqrt{3}}$ comes from simple geometry illustrated in Fig. 1. Of course, Fe_i also polarizes As_{i-x}, As_{i-x-y}, and As_{i-y}. Their polarization vectors are obtained by appropriate rotations from the one just listed.

The interaction Hamiltonian is, then

$$\begin{aligned}\mathcal{H}_{\mathrm{int}} = g\sum_{i,\sigma} \hat{n}_i[&s^\dagger_{i,\sigma}(-\sin\theta p_{i,2,\sigma}+\cos\theta p_{i,3,\sigma})\\ &+ s^\dagger_{i-x,\sigma}(\sin\theta p_{i-x,1,\sigma}+\cos\theta p_{i-x,3,\sigma})\\ &+ s^\dagger_{i-x-y,\sigma}(\sin\theta p_{i-x-y,2,\sigma}+\cos\theta p_{i-x-y,3,\sigma})\\ &+ s^\dagger_{i-y,\sigma}(-\sin\theta p_{i-y,1,\sigma}+\cos\theta p_{i-y,3,\sigma})+\mathrm{h.c.}],\end{aligned} \quad (4)$$

where the sum is over all unit cells i in the lattice. This interaction describes the $s\to p$ transitions and resulting polarization of the As clouds (with the appropriate orientations) if extra charges, counted by $\hat{n}_i=\hat{n}_{i\uparrow}+\hat{n}_{i\downarrow}$, are on Fe_i site. We derive this form explicitly in Appendix A, where we also calculate the strength of the coupling g. Similar models to describe such couplings have been used in Ref. 28.

Our model Hamiltonian $\mathcal{H}=\mathcal{H}_{\mathrm{Fe}}+\mathcal{H}_{\mathrm{As}}+\mathcal{H}_{\mathrm{int}}$ is thus characterized by five parameters, t,t',U_H,Ω,g. We now discuss the choice of their values.

Ab initio calculations[9] find the bandwidth of Fe $3d$ orbitals to be roughly $W=2$ eV. Our hopping model has a bandwidth $W=8t$ irrespective of the value of t', thus $t=0.25$ eV is a typical value. For t', we will consider both the case $t'=0$ and $t'=-t/2=-0.125$ eV, which is the appropriate value for hopping between d_{xy} and the like orbitals which contribute most near the Fermi level. The Hubbard repulsion U_H is certainly a large energy. We will use it as a parameter, and show that our results are very weakly sensitive to its precise value once $U_H>8$ eV or so, which is certain to be the case.

The *ab initio* calculations also suggest a difference from the top of the As $4p$ bands to the bottom of the As $5s$ bands of about 4 eV. This value provides a lower limit for the split Ω between the s and p orbitals. A more appropriate measure would be the distance between the midpoints of these bands, but this is harder to estimate. We use $\Omega=6$ eV as a typical value, and also study the effects of larger Ω values on the results. This is reasonable because higher-energy orbitals of the As will be polarized as well, so one can think of these s and p orbitals as modeling effectively the polarization of the whole atom.

The final parameter needed is g. Since this energy scale characterizes the $s-p$ hybridization when an As polarization cloud is created, we should relate it to the As polarizability α_p. Although we do not know its value precisely, the polarizability is typically equal to the volume of the atom. Since As is a big atom, its polarizability is estimated[9] to be $\alpha_p=10-12$ Å^3.

In Appendix A we show that g equals the product between the typical dipole moment that can be induced on the As ion, ea_{As}, and the electric field created at the As site by the extra

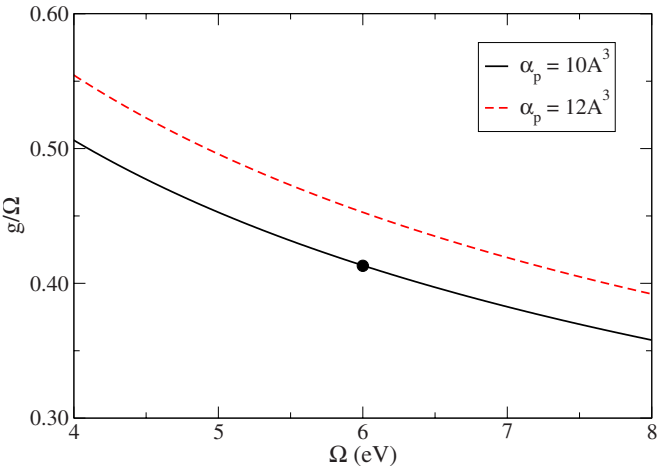

FIG. 3. (Color online) Ratio g/Ω vs Ω, for a fixed polarizability $\alpha_p=10$ Å^3 (full line) and 12 Å^3 (dashed line). The dot indicates our typical choice of parameters.

charge, $E=e/R^2$. Here, a_{As} characterizes the "size" of the s and p orbitals involved [see Eq. (A2)]. On the other hand, a_{As} can be linked to the polarizability since in the linear limit the average induced dipole moment is proportional to the applied field, $\langle p\rangle=\alpha_p E$. The end result derived in Eq. (A11) gives

$$g=\sqrt{\frac{\alpha_p\Omega e^2}{4R^4}}. \tag{5}$$

Using $\alpha_p=10$ Å^3 and $\Omega=6$ eV gives the estimate $g=2.5$ eV and thus $g/\Omega=0.4$, suggesting that nonlinear effects described by our model are starting to become important; however they are not dominant yet.

To conclude, we use $t=0.25$ eV, $t'=0$ or -0.125 eV, $\Omega=6$ eV, and $g=2.5$ eV as typical numbers. We will also allow Ω to vary and we will then choose g according to Eq. (5) so that the polarizability stays constant. The corresponding g/Ω ratio is shown in Fig. 3: for a wide range of values of Ω, g/Ω is roughly 0.4–0.5.

III. SINGLE ELECTRONIC POLARON

We would like to find the eigenstates of the total Hamiltonian $\mathcal{H}=\mathcal{H}_{\mathrm{Fe}}+\mathcal{H}_{\mathrm{As}}+\mathcal{H}_{\mathrm{int}}$ when there is a single extra charge at one of the Fe sites. Of course, it can hop around and will also polarize the As atoms in its vicinity. We call this composite object (the charge dressed by the surrounding polarization clouds) an electronic polaron.

To find its low-energy spectrum, we use perturbation theory in the hopping Hamiltonian. This is a valid approach because t is by far the smallest energy scale in this problem. A more detailed quantitative justification is provided below.

A. Zero-order perturbation

In the absence of hopping the electron will stay at the same site, say at Fe$_i$, and will polarize its four neighbor As, as sketched in Fig. 4. Since we ignore dipole-dipole interactions, we can consider each As ion independently. Consider the state of As$_i$, which is described by

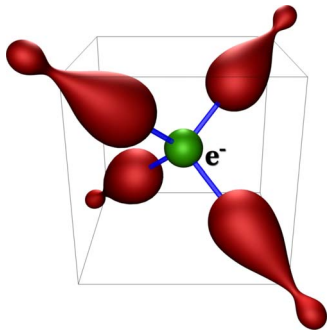

FIG. 4. (Color online) Pictorial illustration of a static electronic polaron. The electron residing on the central Fe atom polarizes the holes on the nn As sites into the $4p$ orbital pointing toward the Fe. More distant As are assumed to remain in the $5s$ ground state.

$$\hat{h}_i=\Omega\sum_{\lambda,\sigma}p^\dagger_{i,\lambda,\sigma}p_{i,\lambda,\sigma}+g\sum_{\sigma}[s^\dagger_{i,\sigma}(-\sin\theta p_{i,2,\sigma}+\cos\theta p_{i,3,\sigma})+\mathrm{h.c}].$$

This quadratic Hamiltonian is trivial to diagonalize. This calculation is detailed in Appendix A, where we find its ground state $E_{\mathrm{cloud}}=\Omega-\sqrt{\Omega^2+4g^2}$, etc.

The ground-state energy of the static polaron is then simply four times larger since it has four polarized As clouds, in other words,

$$E_{P,GS}=4E_{\mathrm{cloud}}=4(\Omega-\sqrt{\Omega^2+4g^2}). \tag{6}$$

The lowest excited state is at $\frac{1}{2}[\Omega+\sqrt{\Omega^2+4g^2}]$ above $E_{P,GS}$, and has either the spin-up or spin-down hole of one of the As atoms polarized in a direction perpendicular to its local electric field. The other excited states are at even higher energies.

The ground state of the polarized As atoms is described by $\gamma^\dagger_{i,\lambda,\pm,\uparrow}\gamma^\dagger_{i,\lambda,\pm,\downarrow}|0\rangle$, where the operators

$$\gamma^\dagger_{i,\lambda,\pm,\sigma}=\cos\alpha s^\dagger_{i,\sigma}-\sin\alpha(\pm\sin\theta p^\dagger_{i,\lambda,\sigma}+\cos\theta p^\dagger_{i,3,\sigma}) \tag{7}$$

are analogs of Eq. (A8) for the specific geometry here. Here $\lambda=1,2$ shows if the in-plane component of the polarization cloud is oriented along axis 1 or axis 2, and the $\pm$ sign indicates whether the in-plane polarization is parallel or antiparallel to this axis. The angle θ is shown in Fig. 1, while α characterizes the mix of p states in the polarization cloud, and is given in Eq. (A9).

Thus, the ground state of the system with the electron at site Fe$_i$ is (since there is a single such electron, its spin is irrelevant and we drop its index here)

$$|\Phi_i\rangle=c^\dagger_i|i\rangle, \tag{8}$$

where $|i\rangle$ describes the state of all As ions,

$$|i\rangle=\prod_{\sigma}\gamma^\dagger_{i,2,-,\sigma}\gamma^\dagger_{i-x,1,+,\sigma}\gamma^\dagger_{i-x-y,2,+,\sigma}\gamma^\dagger_{i-y,1,-,\sigma}|GS\rangle_i, \tag{9}$$

where

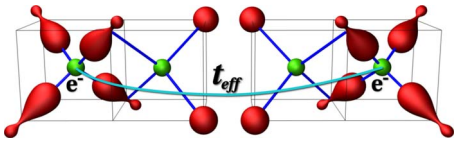

FIG. 5. (Color online) Polaron hopping in the x direction. The hopping integral is renormalized by the overlap between the polarization clouds in the initial and final positions. More distant As are assumed to be in the 5s ground state.

$$|GS\rangle_i = \prod_{|j-i|>R,\sigma} s^\dagger_{j,\sigma}|0\rangle, \tag{10}$$

i.e., it describes unpolarized As ions at all sites which are not nearest neighbor to the site Fe_i containing the extra charge. Thus, the product of γ operators describes the polarization clouds on the four neighbor As sites (both spin-up and spin-down holes are polarized), and $|GS\rangle_i$ describes the remaining holes on the unpolarized As sites. Of course, this ground-state $|\Phi_i\rangle$ is highly degenerate since the electron can be at any Fe site. The hopping lifts this degeneracy.

B. First-order perturbation

In the subspace generated by all the ground states $|\Phi_i\rangle$ described in the previous section, we can form eigenstates which are invariant to translations in the usual fashion,

$$|\Phi_{\vec{k}}\rangle = \sum_i \frac{e^{i\vec{k}\cdot\vec{R}_i}}{N}|\Phi_i\rangle, \tag{11}$$

where the lattice has $N\times N=N^2$ unit cells and we assume periodic boundary conditions. As usual, the quasimomenta $\vec{k}$ are defined inside the first Brillouin zone of the simple square lattice $-\frac{\pi}{a}<k_x,k_y\leq\frac{\pi}{a}$.

Since the hopping Hamiltonian is diagonal in this basis, $\langle\Phi_{\vec{k}}|\hat{T}_{\mathrm{tot}}|\Phi_{\vec{k}'}\rangle\propto\delta_{\vec{k},\vec{k}'}$, it follows that $|\Phi_{\vec{k}}\rangle$ are the eigenstates in first-order perturbation theory. Their energies are

$$E_P(\vec{k}) = E_{P,GS} + \langle\Phi_{\vec{k}}|\hat{T}_{\mathrm{tot}}|\Phi_{\vec{k}}\rangle \tag{12}$$

with the second term describing the polaron dispersion. Straightforward calculation reveals that

$$E_P(\vec{k}) = E_{P,GS} - 2t_{\mathrm{eff}}[\cos(k_x a)+\cos(k_y a)] - 4t'_{\mathrm{eff}}\cos(k_x a)\cos(k_y a) = E_{P,GS} + \epsilon_{\mathrm{eff}}(\vec{k}), \tag{13}$$

in other words the dispersion is identical to that of a free particle, but with renormalized hopping integrals. The renormalization is due to the overlap of the corresponding As clouds as the electron moves from one site to a nearest- or second-nearest-neighbor site, as illustrated schematically in Fig. 5 for the former case, i.e., $t_{\mathrm{eff}}=t\langle i|i+x\rangle$ and $t'_{\mathrm{eff}}=t'\langle i|i+x+y\rangle$. These overlaps result in

$$\frac{t_{\mathrm{eff}}}{t} = \left[\frac{1}{6}\left(1+\frac{\Omega}{\sqrt{\Omega^2+4g^2}}\right)\left(2+\frac{\Omega}{\sqrt{\Omega^2+4g^2}}\right)\right]^4,$$

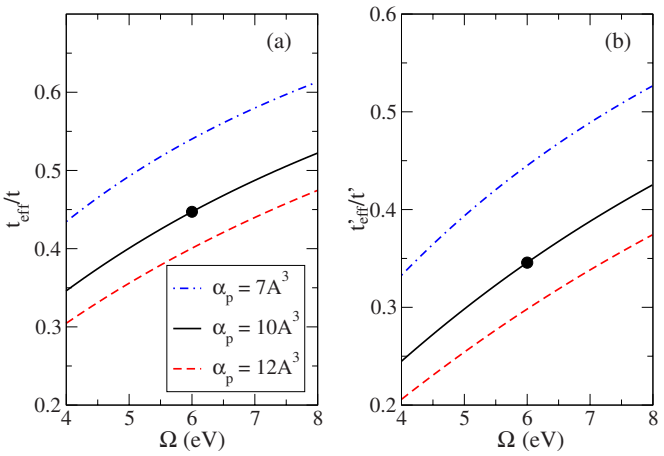

FIG. 6. (Color online) t_{eff}/t (left) and t'_{eff}/t' (right) vs Ω, for different As polarizabilities. The dots indicate the main values used here.

$$\frac{t'_{\mathrm{eff}}}{t'} = \left[\frac{1}{2}\left(1+\frac{\Omega}{\sqrt{\Omega^2+4g^2}}\right)\right]^6\left[\frac{1}{3}\left(1+\frac{2\Omega}{\sqrt{\Omega^2+4g^2}}\right)\right]^2,$$

and are plotted in Fig. 6 vs Ω, for several values of α_p. As expected, in the limit of large Ω, which from Eq. (5) implies $g/\Omega\to 0$, the ratios increase toward unity because the polarization clouds become very small. As Ω decreases, the effective coupling g/Ω increases and the ratios (and therefore the bandwidths) decrease. This is typical polaronic behavior; however note that even if we are in the strong-coupling limit $g/\Omega\to\infty$, the effective hopping is lowered to at most $t_{\mathrm{eff}}/t=1/3^4=0.012$, $t'_{\mathrm{eff}}/t'=1/(2^6 3^2)=0.0017$. While these are, of course, small values, the renormalized hoppings are not becoming exponentially small with increased coupling, as is the case for polarons with phonon clouds. The reason is that within this model, the polarization clouds saturate to a maximum possible value, and therefore the overlap cannot become arbitrarily small.

The effective polaron mass renormalization is inversely proportional to the t_{eff}/t ratio (this statement is exact only if $t'=0$. If t' is finite both ratios determine the new effective mass; however they are roughly equal). Thus, these polarons remain rather light objects, with a mass up to a factor less than 3 larger than the bare band mass. The dots in Fig. 6 indicate our chosen values, for which the polaron mass is roughly 2.2 times the mass of the free band electron, and $t_{\mathrm{eff}}=0.45\times t\approx 0.11$ eV.

While not very large, this renormalization of the effective hoppings/mass further supports our use of the perturbation theory. First-order perturbation is reasonable only assuming that half the effective bandwidth is much smaller than the distance to the next set of excited states, which were ignored in this calculation. As already discussed, those excited states are at $\frac{1}{2}[\Omega+\sqrt{\Omega^2+4g^2}]\approx 6$ eV and higher energies, whereas $4t_{\mathrm{eff}}\approx 0.45$ eV. These numbers suggest that first-order perturbation theory should be quite accurate for parameters in the regime of interest to us (the higher the Ω value used, the more accurate the perturbation theory is). A second-order calculation, which is possible but rather involved, should

only bring in relatively small corrections. Moreover, those corrections may well be of the same order as other ignored small terms (like dipole-dipole interactions between the As clouds), and therefore one would need to reconsider all these approximations carefully before going to a higher order in perturbation theory.

In conclusion, our calculation shows that, to first order, the only effect of the formation of the electronic polarons is to scale down the hopping energy scales by a factor of around 2.5 (with slight differences for nearest vs second nearest-neighbor hopping), but otherwise the dispersion is similar to that predicted by local-density approximation (LDA) for a free charge. Note that this renormalization by a factor of about 2 would also arise in a many-orbital model if the As polarizability is taken into account since the electron's electric field would induce similar As clouds on its neighbors, irrespective of which $3d$ orbital the electron occupies.

Such renormalization of the band structure compared to that predicted by LDA can be detected by angle-resolved photoemission spectroscopy (ARPES). Interestingly, a recent measurement[29] showed reasonable fits to LDA upon rescaling the bandwidth by a factor of 2.2, very similar to our predicted values (the material studied has P instead of As, and these smaller anions have a smaller polarizability $\alpha_p \approx 7$ Å^3). This good agreement is an indication that polaronic effects are important in these materials since such a renormalization is hard to attribute to other physics.

In our model, ARPES would measure a quasiparticle peak at low energies with an $\epsilon_{\text{eff}}(\vec{k})$ dispersion, and a quasiparticle weight

$$Z = |\langle \Phi_{\vec{k}} | c_{\vec{k}}^{\dagger} | GS \rangle|^2 = [\cos \alpha]^{16} \tag{14}$$

independent of momentum (second- and higher-order corrections to the wave functions may bring in some small momentum dependence). For our typical values, this implies $Z = 0.38$. The remaining spectral weight should be observed at much high energies typical of the excited states, of the order $\frac{1}{2}[\Omega + \sqrt{\Omega^2 + 4g^2}] = 6$ eV or more.

IV. BIPOLARON

Within the same model and with the same approximations we now calculate the eigenstates of the system when two charges are present on the Fe sublattice. In particular, we are interested to see whether they become bound into a bipolaron, or whether a state of two free polarons is energetically more favorable.

A. Zero-order perturbation: interaction energies

All the eigenstates of the two charges must be either a singlet or a triplet in the spin space. Since we expect a singlet to be the ground state (this expectation is verified by our calculations) we focus on calculations for singlet eigenstates. The calculations for triplets are very similar; therefore we will only point out where there are differences between the two cases.

Within zero-order perturbation theory the charges cannot move. Depending on the distance between them, different types of polarization clouds can form with different energies. We will now calculate these energies.

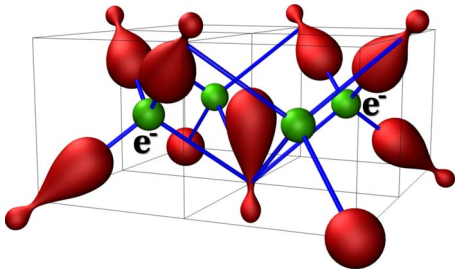

FIG. 7. (Color online) Polarization clouds for a second-nearest-neighbor electronic bipolaron. The central "shared" As atom has a polarization different from that of the usual polaron clouds.

If the two electrons are third-nearest neighbors or further apart, $|i-j| \geq 2a$, then their polarization clouds do not overlap (there is no As atom that is a nearest neighbor to both charged Fe sites). Therefore each charge induces the same four polarization clouds on its four nn As as described for single polarons, and the energy of the pair is simply twice the energy of a polaron,

$$E_{BP,\infty} = 2 \times E_{P,GS} = 8[\Omega - \sqrt{\Omega^2 + 4g^2}]. \tag{15}$$

If the electrons are second-nearest neighbors, they share one As atom, as shown in Fig. 7, so only seven polarization clouds are formed. Six of these are precisely like the ones discussed previously since each of those As ions is in the field created by a single charge. The cloud on the shared As ion, however, is different since it is created by the sum of the electric fields from the two charges. Given the geometry of the system, this new cloud is polarized along the z axis. The only change in calculating the energy and eigenstate of this cloud is to replace $g \to 2g \cos\theta = 2g/\sqrt{3}$ in Eq. (A5) to reflect the increased applied electric field. As a result, the energy of this cloud is changed to $\Omega - \sqrt{\Omega^2 + \frac{16}{3}g^2}$, and therefore the total energy of the second nearest-neighbor static bipolaron is

$$E_{BP,2} = 6[\Omega - \sqrt{\Omega^2 + 4g^2}] + \left[\Omega - \sqrt{\Omega^2 + \frac{16}{3}g^2}\right].$$

This energy is different from the energy of two free polarons by an amount

$$U_2 = E_{BP,2} - E_{BP,\infty} = 2\sqrt{\Omega^2 + 4g^2} - \Omega - \sqrt{\Omega^2 + \frac{16}{3}g^2}. \tag{16}$$

This is plotted in Fig. 8(c) vs Ω, for three values of As polarizability. It is a slowly varying function of Ω and positive, meaning that it is energetically more favorable to have two free electronic polarons situated far apart than to have them on second-nearest-neighbor sites. This can be shown to be true for any value of the α_p and Ω (i.e., any g/Ω ratio), for this lattice structure.

The reason for this repulsion, at least in the linear regime $g/\Omega \ll 1$, is directly linked to the geometry of the problem. In this limit, the charge-dipole energy for the As which is neigh-

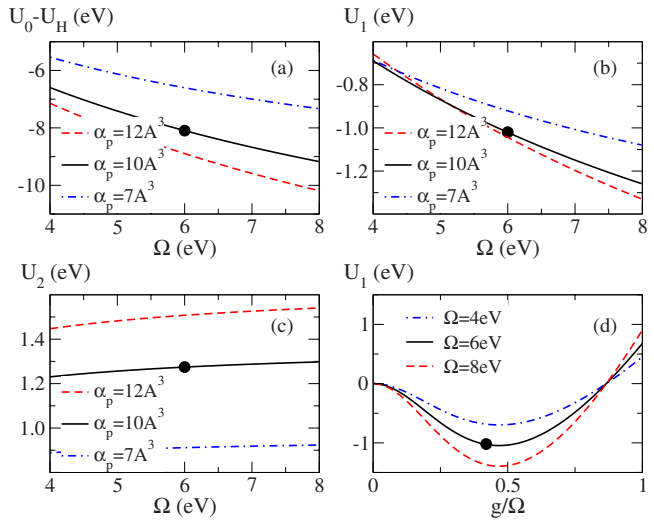

FIG. 8. (Color online) (a) Renormalization of on-site interaction, U_0-U_H; (b) nn energy U_1 and (c) second-nn energy U_2 vs Ω for various polarizabilities. (d) U_1 vs g/Ω when $\Omega=4,6,8$ eV. The dots show our typical values.

bor to both charged Fe sites is $-\alpha_p(\vec{E}_1+\vec{E}_2)^2/2$, where $\vec{E}_1,\vec{E}_2$ are the electric fields created by the two charges. The energy difference with respect to two regular clouds is $-\alpha_p\vec{E}_1\cdot\vec{E}_2$. This implies a repulsive interaction if the Fe-As-Fe angle is larger than 90°, as is the case here. This also shows that this term can turn attractive if the lattice is distorted so as to make this angle sharp. In terms of the angle θ shown in Fig. 1, this requires that $2\cos^2\theta>1\rightarrow\theta<45°$ and can be achieved by making the lattice tetragonal, i.e., by increasing the distance between the Fe and As layers by a factor of $\sqrt{2}$ or more. Of course, this lattice deformation would also have the added effect of decreasing all the polarization energies since the electric fields would be smaller due to the increased Fe-As distances.

This argument demonstrates that if the Fe-As-Fe angle is less than 90°, the interaction becomes attractive. This is the case if the two charges are on nearest-neighbor Fe sites, or on the same Fe, as pointed out in Ref. 9.

Indeed, consider the nearest-neighbor bipolaron. In this case, as illustrated in Fig. 9, a total of six As atoms are polarized. Four of them have clouds of the original type, while two, which are neighbors to both Fe atoms, have yet another type of polarization cloud which lies in the plane perpendicular to be bipolaron axis. Straightforward geometry arguments shows that the electric fields at these sites is $\sqrt{\frac{8}{3}}$ larger than e^2/R; therefore one has to replace $g\rightarrow g\sqrt{\frac{8}{3}}$ to find the energy of each new cloud.

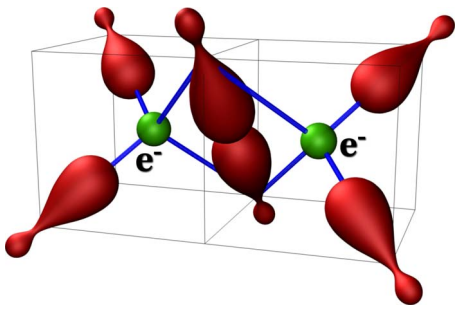

FIG. 9. (Color online) Polarization clouds for a nearest-neighbor electronic bipolaron. The two central "shared" As atoms have a polarization different from that of the usual polaron clouds.

Thus, the total energy of a static nearest-neighbor bipolaron is

$$E_{BP,1}=4[\Omega-\sqrt{\Omega^2+4g^2}]+2\left[\Omega-\sqrt{\Omega^2+\frac{32}{3}g^2}\right],$$

and the difference to the energy of two free polarons is

$$U_1=E_{BP,1}-E_{BP,\mathrm{inf}}=4\sqrt{\Omega^2+4g^2}-2\Omega-2\sqrt{\Omega^2+\frac{32}{3}g^2}. \tag{17}$$

This effective energy is plotted in Fig. 8(b) as a function of Ω for a fixed polarizability and in Fig. 8(d) as a function of g/Ω for several values of Ω.

The first observation is that this effective interaction is indeed attractive, favoring a bound nearest-neighbor bipolaron over two independent polarons. As shown in Fig. 8(d), this is only true for small $g/\Omega<1$ values, however, with the nonlinear effects making the interaction repulsive at large g/Ω values. Remarkably, the strongest binding energy is for $g/\Omega\approx0.45$ for reasonable values of Ω, which is close to the values we expect for this ratio (see Fig. 3). From this point of view, we can say that these lattices are already very close to being fully optimized. As for the case of the second nn bipolaron, it is possible to further change this interaction by changing the lattice geometry: a smaller θ angle will increase this binding energy, but this is balanced by a loss if the Fe-As distance is increased.

The analysis so far would be identical if the bipolarons were in a triplet state. The last case—the onsite bipolaron—is only possible for a singlet state. In this configuration there are again four polarization clouds, like for a single polaron. However, because the charge is doubled so are the electric fields, and we replace $g\rightarrow2g$. As a result, the energy of the on-site bipolaron is

$$E_{BP,0}=4[\Omega-\sqrt{\Omega^2+16g^2}],$$

and the effective on-site interaction is

$$\begin{aligned}U_0&=U_H+E_{BP,0}-E_{BP,\infty}\\&=U_{\mathrm{H}}-4[\sqrt{\Omega^2+16g^2}+\Omega-2\sqrt{\Omega^2+4g^2}]<U_H.\end{aligned} \tag{18}$$

Clearly, the polarization of neighboring As atoms always acts to screen out the on-site repulsion, and this effect can be very significant. Indeed, in Fig. 8(a) we plot this renormalization energy, which is several eV for typical parameters of interest to us. In the linear regime, this renormalization energy would be $\approx-16g^2/\Omega\approx-16$ eV, which is similar to the values found in Ref. 9. The smaller values we find here are a direct consequence of the nonlinear effects, which are accounted for in our model.

Such on-site screening is well known to arise in polaron models.[21,22,32] For pnictides, it could well be the main reason why they are not in the strongly coupled $U_0 \gg t$ regime. However, the nearest-neighbor attraction *is not* typical polaron physics. On a 2D lattice like in cuprates, the nn interaction between electronic polarons is *repulsive* because the Cu-O-Cu angle is 180° (the same holds true for polarons coupled to a breathing-mode phonon of the O atoms). For a Holstein bipolaron, there is a weak nn attraction, but it is due to spin exchange and is $\mathcal{O}(t^2)$, not $\mathcal{O}(t^0)$ like here.[21,31] Its particular non-2D geometry is the essential ingredient in bringing about this strong nn attraction, for the pnictides. This mechanism is impossible in cuprates.

To summarize, this calculation reveals that for the parameters of interest to us, we can have a stable on-site bipolaron if the Hubbard repulsion is not too large. The nearest-neighbor bipolaron is bound, whereas the second nearest-neighbor bipolaron is unstable to dissociation into two free polarons.

B. First-order perturbation

We continue the discussion for singlet bipolarons, and analyze how the hopping Hamiltonian mixes together the low-energy bipolaron states $s^\dagger_{i,i+\vec{\delta}}|i,i+\vec{\delta}\rangle$, where $s^\dagger_{i,i+\vec{\delta}} = \frac{1}{\sqrt{2}}(c^\dagger_{i\uparrow}c^\dagger_{i+\vec{\delta}\downarrow} - c^\dagger_{i\downarrow}c^\dagger_{i+\vec{\delta}\uparrow})$ if $\delta \neq 0$, and $s^\dagger_{ii} = c^\dagger_{i\uparrow}c^\dagger_{i\downarrow}$ describes the singlet. Here, $\vec{\delta}$ measures the distance between the two charges, and $|i,i+\vec{\delta}\rangle$ describes the As atoms when there are charges at Fe sites i and $i+\vec{\delta}$. Similar to the states $|i\rangle$ defined for single polarons, the states $|i,i+\vec{\delta}\rangle$ have all As atoms which are not nearest neighbors to either Fe_i or $\mathrm{Fe}_{i+\vec{\delta}}$ in their unpolarized ground state, while the As atoms nn to the charged Fe atoms are described by the appropriate $\gamma^\dagger$, $\tilde{\gamma}^\dagger$, $\tilde{\tilde{\gamma}}^\dagger$, or $\tilde{\tilde{\tilde{\gamma}}}^\dagger$ operator, as detailed in Appendix B. We do not list these expressions explicitly here, as they are rather long and tedious but otherwise straightforward.

From these states, we can define a basis of bipolaron states invariant to translations on the $N \times N$ unit cells lattice,

$$|\vec{k},\vec{\delta}\rangle = \sum_i \frac{e^{i\vec{k}\cdot(\vec{R}_i+\vec{\delta}/2)}}{N} s^\dagger_{i,i+\vec{\delta}}|i,i+\vec{\delta}\rangle. \tag{19}$$

Here $\vec{k}$ is the center-of-mass momentum of the pair. It can take the usual values inside the Brillouin zone allowed by the periodic boundary conditions. Care needs to be taken in choosing the set of $\vec{\delta}$ values since if we take all its possible values, we double count (e.g., $|\vec{k},\vec{e}_x\rangle = |\vec{k},-\vec{e}_x\rangle$, etc). This is due to the fact that $\vec{\delta}$ is like a nematic vector, with a size and orientation but without a pointing arrow. Let $\vec{\delta} = \delta_x\vec{e}_x + \delta_y\vec{e}_y$, and for simplicity assume that the lattice size is an odd number, $N = 2n+1$. Then, double counting is avoided provided that when $\delta_x = 0$, we allow $\delta_y = 0,1,\ldots,n$ (because of the periodic boundary conditions, the distance between charges cannot be more than half the dimension of the system). If $\delta_x = 1,2,\ldots,n$, then $\delta_y = -n,\ldots,n$. Both positive and negative values are needed in this case because, for example, the $|\vec{k},\vec{e}_x+\vec{e}_y\rangle$ state is distinct from the $|\vec{k},\vec{e}_x-\vec{e}_y\rangle$ state; however these are the only two distinct states of the second nearest-neighbor bipolarons. In conclusion, for a $N \times N$ lattice with $N = 2n+1$, there are $(n+1)(2n+1)-n$ distinct singlet eigenstates corresponding to a given total momentum $\vec{k}$. The remaining states are triplet states. Similar accounting can be done for lattices with even number of sites N.

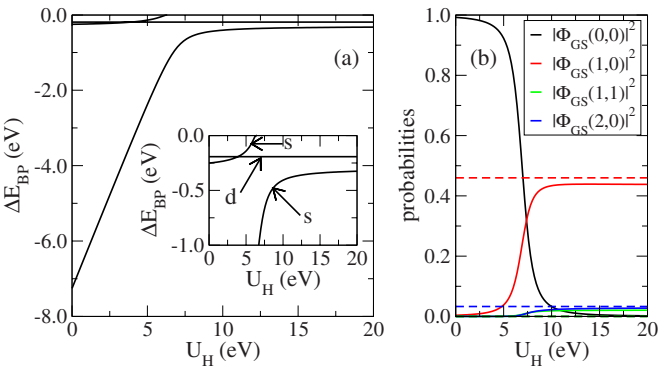

FIG. 10. (Color online) (a) Bound eigenstates measured from the two-polaron continuum, $\Delta E_{BP} = E_{BP}(0) + 8t_{\mathrm{eff}}$ vs U_H. The symmetry of the eigenstates is labeled in the inset. (b) Probability for on-site, first-, second-, and third-nn separations in the ground state, vs U_H. The dashed lines show the same quantities for the d state. Here $t' = 0$, $\alpha_p = 10$ Å^3, $\Omega = 6$ eV (similar results are found for all $\alpha_p = 7-12$ Å^3, $\Omega = 4-8$ eV).

Because our total Hamiltonian is also invariant to translations, it will not mix states with different total momenta. Therefore, we can solve the problem separately in each $\vec{k}$ subspace, and only need to calculate the various $\langle\vec{k},\vec{\delta}'|\mathcal{H}|\vec{k},\vec{\delta}\rangle$ matrix elements. There are three sets of contributions. First, there are diagonal matrix elements, already discussed in the previous section. Specifically, $\langle\vec{k},\vec{\delta}|\mathcal{H}|\vec{k},\vec{\delta}\rangle = \langle\vec{k},\vec{\delta}|\hat{U} + \mathcal{H}_{\mathrm{As}} + \mathcal{H}_{\mathrm{int}}|\vec{k},\vec{\delta}\rangle = U_{\vec{\delta}}$, where U_0, U_1, and U_2 of Eqs. (18) and (19) correspond to $\vec{\delta}$, indicating, respectively, an on-site, a nearest-neighbor, or a second-nearest-neighbor bipolaron state. If $|\vec{\delta}| \geq 2$, then $U_{\vec{\delta}} = 0$ since we measure the interactions energies with respect to the energy of two unbound static polarons.

The nn hopping Hamiltonian links states with the same momentum but bipolaron distances $\vec{\delta}$ and $\vec{\delta}'$ which are nearest neighbor, i.e., $|\vec{\delta}-\vec{\delta}'| = 1$. We therefore also need to calculate these matrix elements $\langle\vec{k},\vec{\delta}\pm\vec{e}_{x/y}|\mathcal{H}|\vec{k},\vec{\delta}\rangle = \langle\vec{k},\vec{\delta}\pm\vec{e}_{x/y}|\hat{T}|\vec{k},\vec{\delta}\rangle$. Similarly, for finite t' there are matrix elements of $\hat{T}'$ between second-nearest-neighbor states with $|\vec{\delta}-\vec{\delta}'| = \sqrt{2}$. All these matrix elements and the resulting effective hoping integrals are calculated in Appendix B. Taken together, these three sets exhaust all matrix elements which are finite, and therefore we can diagonalize the resulting matrix and find the energies $E_{BP}(\vec{k})$ and eigenstates corresponding to any desired momentum $\vec{k}$ of the bipolaron, within first-order perturbation theory.

We begin by analyzing results when $t' = 0$. In Fig. 10(a) we plot $\vec{k} = 0$ energies for all bound bipolaron states, i.e., those lying below the two-polaron continuum starting at $-8t_{\mathrm{eff}}$. We find three such states. The ground-state energy first increases linearly with U_H and then flattens out. Its wave

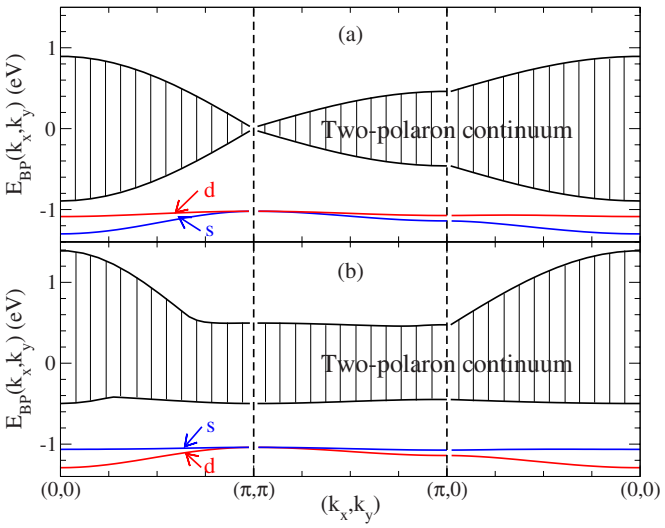

FIG. 11. (Color online) Dispersion of bound bipolaron states along high-symmetry axes in the Brillouin zone, for (a) $t'=0$ and (b) $t'=-t/2$. The two-polaron continuum is also shown. Parameters are $U_H=10$ eV, $\alpha_p=10$ Å^3, $\Omega=6$ eV (similar results are found for all $\alpha_p=7-12$ Å^3, $\Omega=4-8$ eV). The symmetry of the ground state changes from s to d if $t'\neq 0$.

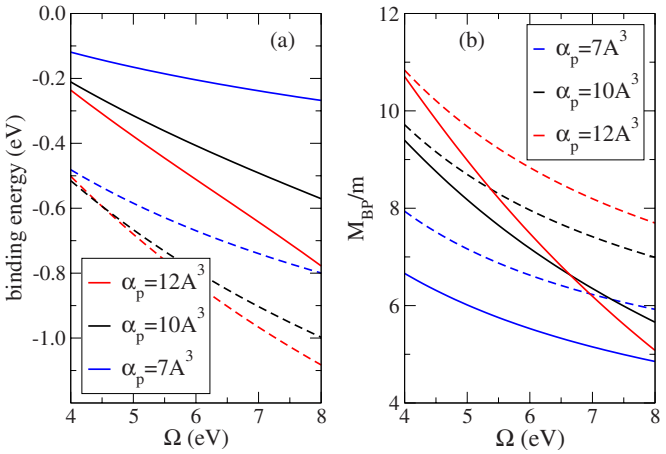

FIG. 12. (Color online) Ground-state bipolaron (a) binding energy, and (b) effective mass in units of the free-carrier mass vs Ω, for various polarizabilities. The full lines correspond to $t'=0$, dashed lines to $t'=-t/2$. Here $U_H=10$ eV.

function has s-type symmetry (its sign is unchanged upon 90° rotation). There is a second weakly bound s state at small U_H, which then joins the continuum. The third bound bipolaron state has an energy independent of U_H, and is d type (wave function changes sign upon 90° rotation).

The nature of these bound states is revealed in Fig. 10(b). For low U_H values, the ground state primarily consists of an on-site bipolaron, with hardly any contribution from nn or more distant configuration. This explains why its energy here scales with U_H (more precisely with U_0). When $U_0\approx 0$ there is a fast crossover to a state dominated by the nn bipolaron configurations (a combined total of 90% probability). This is expected since $U_1<0$ irrespective of U_H, favoring such a pair when U_0 becomes repulsive. The on-site contribution is now exponentially small. This explains the weak U_H dependence here, as coming from virtual hopping to the on-site configuration. The dashed lines show the contributions for the d-type state. As expected, it is dominated by nn bipolarons. It has a zero on-site probability, consistent with its symmetry and explaining the lack of dependence on U_H. The second nn contribution is also zero ($U_2>0$ as well). There are small third and more distant bipolaron contributions.

The unscreened Hubbard repulsion is very large, $U_H\sim 10-20$ eV. For such values our results show hardly any dependence on U_H, so its precise value is of little importance. We use $U_H=10$ eV from now, and ask how mobile are these bound, predominantly nn, bipolaron pairs. Their dispersion in the Brillouin zone in shown in Fig. 11(a), where we also show the two-polaron continuum (eigenstates above the continuum are not shown). The s pair has a bandwidth $E_{GS}(\pi,\pi)-E_{GS}(0,0)\approx 0.3$ eV, implying a *bipolaron mass about seven times that of a free-carrier mass* (the bandwidth of a free electron is $8t=2$ eV). This is a very small enhancement, since it means that the bipolaron is about 3.5 times heavier than a single polaron. In Fig. 12(b) we plot the bipolaron mass for various α_p and Ω values, showing only limited variation over a wide parameter range. The higher-energy d pair is heavier, with a much narrower bandwidth.

If we include second nn hopping $t'=-t/2$, two effects are apparent in Fig. 11(b). First, the two-polaron continuum is pushed to higher energies, effectively increasing the binding energies of the bipolarons. [The binding energies for the ground-state bipolaron are shown in Fig. 12(a) for various parameters]. Second, the d state becomes the ground state. This is not surprising since the second nn hopping links directly the two nn bipolaron configurations which give the bulk contribution to these eigenstates. For $t'<0$, this mixing raises the energy of an s state and lowers that of a d state. Thus, if the effective t' between the two nn bipolaron configurations is large enough, the d state has to become the ground state.

Let us now comment briefly on the triplet eigenstates. Since there is no onsite triplet bipolaron configuration, their energies are essentially identical to the energies of the singlet eigenstates in the limit $U_H\to\infty$. This implies that at this level of approximation and for large enough U_H, singlet and triplet bound bipolarons are almost degenerate. However, it is well known that second-order perturbation theory produces an exchange interaction which strongly favors the singlet eigenstates (this is the interaction responsible for the weak binding of the S1 Holstein bipolaron[32]). It follows that in reality, the ground state must be a singlet.

V. DISCUSSION AND SUMMARY

The binding energies shown in Fig. 12(a) are substantial, even without the addition of this singlet exchange energy. As discussed in Appendix C, relaxation of our approximations (that only As ions nn to a charge are polarized and that dipole-dipole interactions are ignored) further enhances U_1, and therefore these binding energies, to several eV. Yet more enhancement is expected if we include even higher orbitals than $5s$ when describing the As ion polarization. All this

suggests the appearance of preformed bipolaron pairs well above room temperature. On the other hand, in our model Hamiltonian we have ignored a nn repulsion energy which comes from the bare Coulomb interaction itself (in reality, this nn Coulomb repulsion will be reduced by other screening mechanisms, such as the bond polarizabilities involving the As $4p$ and Fe $3s$ and $4p$ states). This nn repulsion will decrease U_1 substantially, and may even change its sign, making nn bipolaron pairs unstable. It is difficult to obtain accurate quantitative estimates of all these terms, to find out whether bound bipolaron states exist and what are their binding energies.

It is important to point out that the presence of this As-mediated large-nn attractive interaction U_1 may be essential even if preformed bipolaron pairs do not exist. This would put these materials in a BCS-like framework, with the phonon glue replaced by a virtual excitonic glue. Because in our model U_1 is so large and the effective masses are so small one does not really need much of a retardation effect to overscreen the bare nn Coulomb repulsion. This is unlike in any other models, such as the Little and ABB models, which envision a similar type of glue. In favor of this BCS-like scenario is experimental data indicating higher T_c in samples with shorter Fe-As distances and smaller Fe-As-Fe angles, which is precisely what increases U_1. We also note that since the unbound polarons are fermions, appearance of magnetic order such as a spin-density wave (SDW) at low concentrations is not inconsistent with our model. In fact, their enhanced mass would, if anything, rather favor such an ordered magnetic state.

However we do not want to rule out the presence of preformed pairs of the kind discussed above. There is ample evidence that singlet pairs may exist to quite high T in these systems. For example, the magnetic susceptibility[30] shows the same strong increase with T both above the SDW and the superconducting phase. This is very difficult to explain starting from a free single-particle picture, but easy to understand if we assume the presence of preformed singlet pairs well above T_c, with a binding energy of the order of 100 meV or more. The magnetic susceptibility of such a system would increase with increasing T with an activated kind of behavior, in agreement with NMR Knight-shift data.[31]

We therefore suggest to take the scenario of preformed singlet bipolarons seriously. We note that a superconducting state would then behave more like a Bose Einstein condensate. At first glance one might think that its T_c would have to be very low; however we note that these bipolarons are very light, with a mass which is about 3–4 times the single polaron mass, and thus high condensation temperatures could be expected. The other rather interesting aspect to consider is that perhaps this scenario might also explain the low amplitude SDW observed at low dopings, as being a different kind of condensate of singlet bipolarons due to the rather strong exchange interactions. The low amplitude would be a result of the pairwise singlet formation tendency competing with the pair-pair exchange interactions which would favor the SDW. We propose to study these issues next.

To conclude, we argue that the polarizability of the anions plays a very important role in these materials. Excess charges at Fe sites are "dressed" by polarization clouds on nearby As anions. As a result, the fermionic quasiparticles are electronic polarons, with somewhat enhanced effective masses. If this was all, one could "forget" about this physics in a similar way to cuprates, where as long as the correct t and U parameters are used one generally ignores the fact that quasiparticles are really Zhang-Rice singlets, with significant O anion contributions. However, because of the large polarizability and the geometry of the lattice, we find a strong suppression of the on-site repulsion, which explains (at least partially) why these materials are not strongly correlated. More importantly, a significant eV-range nearest-neighbor attraction arises between these polarons, and must play a role in the pairing in these materials. Whether it is sufficient on its own to describe superconductivity or whether additional attraction mechanisms need to be found remains an open question. We believe, however, that these effects are too large to be irrelevant.

ACKNOWLEDGMENTS

We thank J. Zaanen, J. van den Brink, C. Varma, D. Bonn, and A. Damascelli for many stimulating discussions and insightful opinions. This work was supported by NSERC and by CIfAR Nanoelectronics and Quantum Materials. Part of this work was carried out at the Kavli Institute for Theoretical Physics, which is supported by NSF under Grant No. PHY05-51164.

APPENDIX A: THE CHARGE-DIPOLE INTERACTION TERM

Consider the polarization cloud formed on an As ion due to a charge q placed at a distance R away, in the direction characterized by the vector $\vec{e}$. The electric field at the As site is then $\vec{E}=\frac{q}{R^2}\vec{e}$. Note that we use an unscreened value for this electric field. The reason is that we are interested in behavior related to the high-frequency dynamic electronic polarizability, and not that due to slow vibrational motion of the As themselves. As we demonstrated here, the effective masses of the polarons and bipolarons are fairly small, meaning that they are highly mobile. The As ions are fast to acquire a polarization cloud, but since they are very heavy, they simply cannot move quickly enough to follow the fast polaron dynamic. This separation of energy scales allows us to ignore lattice dynamics effects in the following.

The interaction between the As and the electric field is $\mathcal{H}_{\text{int}}=-\hat{\vec{p}}\cdot\vec{E}$, where $\hat{\vec{p}}$ is the As dipole moment operator. In the second quantization, and if we restrict ourselves only to s and p orbitals to describe the relevant As states, its dipole moment is

$$\hat{\vec{p}}=\sum_{\lambda,\sigma}\langle s|e\vec{r}|p_\lambda\rangle(s_\sigma^\dagger p_{\lambda,\sigma}+\text{h.c.}), \tag{A1}$$

where $\lambda=x,y,z$ or $\lambda=1,2,3$, and we already took in consideration the fact that there are no matrix elements of the dipole moment between orbitals of the same type ($\langle s|\vec{r}|s\rangle=0$, etc). Moreover, $\langle s|e\vec{r}|p_\lambda\rangle=e\vec{e}_\lambda a_{\text{As}}$ since the operator $\vec{r}$ has a nonvanishing matrix element only in the direction $\vec{e}_\lambda$ of the

orbital p_λ involved. Thus, a_{As} is a characteristic "size" of the ion, defined as

$$a_{\mathrm{As}} = \langle s|x|p_x\rangle = \int d\vec{r}\phi_x^*(\vec{r})x\phi_{p_x}(\vec{r}) = \langle s|y|p_y\rangle = \langle s|z|p_z\rangle. \tag{A2}$$

Therefore, we find

$$\mathcal{H}_{\mathrm{int}} = -\frac{ea_{\mathrm{As}}q}{R^2}\sum_{\lambda,\sigma}(\vec{e}\cdot\vec{e}_\lambda s_\sigma^\dagger p_{\lambda,\sigma} + \mathrm{h.c.}). \tag{A3}$$

This is exactly the form used in Eq. (4), except there we have explicitly written the various projections $\vec{e}\cdot\vec{e}_\lambda$ in terms of the angle θ appropriate for our geometry, and summed over all As anions. It follows that $g=-ea_{\mathrm{As}}q/R^2$. If the charge producing the electric field is a single electron then $q=-e$, so that

$$g = \frac{a_{\mathrm{As}}e^2}{R^2}. \tag{A4}$$

This shows that g is an energy equal to the typical induced dipole ea_{As} times the applied electric field e/R^2. We now connect this quantity to the anion polarizability.

For simplicity, for the rest of this section let us denote $p_\sigma=\Sigma_\lambda\vec{e}\cdot\vec{e}_\lambda p_{\lambda,\sigma}$, i.e., it is the annihilation operator for the p orbital oriented in the direction $\vec{e}$ of the applied electric field. Of course, one can form two other linear combinations of the p_x,p_y,p_z orbitals which are orthogonal to this direction. These two do not couple to the electric field and do not participate in the polarization cloud, thus their energetics is trivial. The interesting part for the problem of the As cloud in the presence of the extra charge is therefore described by the Hamiltonian

$$\hat{h} = \Omega\sum_\sigma p_\sigma^\dagger p_\sigma + g\sum_\sigma (s_\sigma^\dagger p_\sigma + \mathrm{h.c.}). \tag{A5}$$

This Hamiltonian is trivial to diagonalize. Its ground state has the energy

$$E_{\mathrm{cloud}} = \Omega - \sqrt{\Omega^2 + 4g^2} \tag{A6}$$

and the eigenstate

$$|GS\rangle = \gamma_\uparrow^\dagger\gamma_\downarrow^\dagger|0\rangle, \tag{A7}$$

where

$$\gamma_\sigma^\dagger = \cos\alpha s_\sigma^\dagger - \sin\alpha p_\sigma^\dagger \tag{A8}$$

and

$$\cos\alpha = \sqrt{\frac{1}{2}\left(1+\frac{\Omega}{\sqrt{\Omega^2+4g^2}}\right)}. \tag{A9}$$

The angle $\alpha<90°$ characterizes the admixture of excited p hole states in the ground state in the presence of the electric field, and thus the degree of polarization of the anion. Indeed, note that if $g=0$ (no electric field) this is reduced to the expected As unpolarized ground state (holes in the s orbitals, $\alpha=0°$) whereas for $g\to\infty$, the γ operators describe the maximally polarized orbital $(s-p_x)/\sqrt{2}$, $\alpha=45°$.

The second eigenstate of $\hat{h}$ has an energy $E_{\mathrm{exc}}=\Omega+\sqrt{\Omega^2+4g^2}$ and corresponds to filling up the orbitals $\eta_\sigma^\dagger=\sin\alpha s_\sigma^\dagger+\cos\alpha p_\sigma^\dagger$, i.e., of creating a polarization cloud oriented antiparallel to the electric field. As already discussed, one can also excite the hole in the p orbitals orthogonal to the direction of the electric field, with energy Ω. Given that Ω is a large energy, all these excited states are well above the ground state.

Finally, the dipole moment induced on the As atom is

$$\langle p\rangle = \langle GS|\vec{e}\cdot\hat{\vec{p}}|GS\rangle = \frac{4ea_{\mathrm{As}}g}{\sqrt{\Omega^2+4g^2}}. \tag{A10}$$

Since Eq. (A4) revealed that g is proportional to the applied electric field $E=e/R^2$, this shows that in the linear limit $g\ll\Omega$ we can approximate

$$\langle p\rangle \approx \frac{4ea_{\mathrm{As}}g}{\Omega} = \frac{4e^2a_{\mathrm{As}}^2}{\Omega}E$$

and thus identify the polarizability from this linear regime where $\langle p\rangle=\alpha_pE$. This allows us to extract a_{As} in terms of α_p and then, through Eq. (A4), to calculate

$$g^2 = \frac{\alpha_p\Omega e^2}{4R^4}. \tag{A11}$$

Using $\alpha_p=10$ Å^3 and $\Omega=6$ eV gives the estimate $g=2.5$ eV and thus $g/\Omega=0.4$, suggesting that nonlinear effects described by our model are starting to become important; however they are not dominant yet. For example, with these numbers, the energy of the polarized As cloud from Eq. (A6) is $E_{\mathrm{cloud}}=-1.78$ eV, whereas in the linear regime $g/\Omega\ll1$ we would have $E_{\mathrm{cloud}}\approx-\frac{2g^2}{\Omega}=-2.05$ eV. As a consistency check, also note that the linear expression for the energy of the cloud can be rewritten as $E_{\mathrm{cloud}}\approx-\frac{2g^2}{\Omega}=-\frac{\alpha_pE^2}{2}$, as expected to be the case in this linear regime.[9]

APPENDIX B: BIPOLARON RESULTS

1. Polarization cloud operators

For completeness, we list here the operators which describe the polarization clouds for the As atoms which are nn to both charged Fe sites, for second-nn, nn, and on-site bipolarons. These are the analogs of Eqs. (A8) and (A9) for the electric fields appropriate for each case.

For a second-nn configuration, if the As which is nn to both charged Fe sites is As$_i$, then its ground state is described by $\tilde{\gamma}_{i\uparrow}^\dagger\tilde{\gamma}_{i\downarrow}^\dagger|0\rangle$, where

$$\tilde{\gamma}_{i,\sigma}^\dagger = \cos\beta s_{i,\sigma}^\dagger - \sin\beta p_{i,3,\sigma}^\dagger, \tag{B1}$$

and

$$\cos\beta = \sqrt{\frac{1}{2}\left(1+\frac{\Omega}{\sqrt{\Omega^2+\frac{16}{3}g^2}}\right)} \tag{B2}$$

with $\beta<90°$.

For a nn bipolaron, the creation operators for the polarization clouds of the central As ions are

$$\tilde{\tilde{\gamma}}^{\dagger}_{i,\pm,\sigma} = \cos\ \gamma s^{\dagger}_{i,\sigma} - \sin\ \gamma \frac{\pm p^{\dagger}_{i,\lambda,\sigma} + p^{\dagger}_{i,3,\sigma}}{\sqrt{2}}, \tag{B3}$$

where $\lambda = x$ or y is the direction perpendicular to the bipolaron axis, and the $\pm$ sign shows whether the cloud is parallel/antiparallel to the λ axis. The new mixing angle is

$$\cos\ \gamma = \sqrt{\frac{1}{2}\left(1 + \frac{\Omega}{\sqrt{\Omega^2 + \frac{32}{3}g^2}}\right)} \tag{B4}$$

with $\gamma < 90°$.

Finally, the cloud operators for the on-site bipolaron are similar to the original polaron cloud operators

$$\tilde{\tilde{\gamma}}^{\dagger}_{i,\lambda,\pm,\sigma} = \cos\ \delta s^{\dagger}_{i,\sigma} - \sin\ \delta[\pm \sin\ \theta p^{\dagger}_{i,\lambda,\sigma} + \cos\ \theta p^{\dagger}_{i,3,\sigma}], \tag{B5}$$

where $\lambda = 1$ or 2 depending on the in-plane alignment of the cloud, and $\pm$ reflects its orientation. The only difference is the new mixing angle $\delta < 90°$, where

$$\cos\ \delta = \sqrt{\frac{1}{2}\left(1 + \frac{\Omega}{\sqrt{\Omega^2 + 16g^2}}\right)}. \tag{B6}$$

2. Matrix elements of the hoping Hamiltonian

If the separation $\vec{\delta}$ between the two excess charges is large enough, the hopping Hamiltonian $\hat{T}$ will hop one of the electrons away from its clouds, while the second one remains unperturbed. As a result, one expects the matrix element to be proportional to the t_{eff} of the single polaron. Indeed, explicit calculation shows that if the separation $\vec{\delta}$ is at least that of a third nearest-neighbor bipolaron, then

$$\langle \vec{k}, \vec{\delta} + \vec{e}_x | \hat{T} | \vec{k}, \vec{\delta} \rangle = -2t_{\text{eff}} \cos\frac{k_x a}{2},$$

$$\langle \vec{k}, \vec{\delta} \pm \vec{e}_y | \hat{T} | \vec{k}, \vec{\delta} \rangle = -2t_{\text{eff}} \cos\frac{k_y a}{2}. \tag{B7}$$

The cosine factors appear because of the phases in the definitions of the eigenstates $|\vec{k}, \vec{\delta}\rangle$, which change when the singlet separation $\vec{\delta}$ changes. Given the restrictions on the allowed values of $\vec{\delta}$, one needs to be a bit careful near the boundary of allowed values. For example, based on the definition of Eq. (21), it is straightforward to check that

$$|\vec{k}, \delta_x \vec{e}_x + (n+1)\vec{e}_y\rangle = e^{ik_y a(2n+1)/2} |\vec{k}, \delta_x \vec{e}_x - n\vec{e}_y\rangle.$$

Given the periodic boundary conditions, the allowed values for momentum, if $N = 2n+1$, are $k_y a = 2\pi n_y/(2n+1)$, and the phase factor linking the two states can only be ± 1. This sign is important because hopping in the y direction links the state with $\delta_y = n$ to that with $\delta_y = n+1$; however the later one is not among the allowed $\vec{\delta}$ values. The identity above links it to an allowed value, but also introduces a phase shift (the sign) which is transferred to the corresponding matrix element. A similar situation arises for hopping in the x direction when $\delta_x = n$, $\delta_x = 0$ and hopping in the y direction for $\delta_y = -n$. Finally, it is important to note that these phase shifts are different for triplet states (they have opposite sign in most, but not all cases). Other than this (and the nonexistence of an triplet onsite bipolaron, as already discussed), essentially everything else is the same in the calculation for triplet states.

Different effective hopping integrals appear when the electrons are closer together. For nearest-neighbor hopping, there are four such special cases. The first corresponds to hopping from third-nearest-neighbor to nearest-neighbor bipolaron. A straightforward calculation of the overlap of the corresponding polarization clouds leads to an effective hopping

$$\frac{t_3}{t} = \langle i, i + \vec{e}_x | i, i + 2\vec{e}_x \rangle$$
$$= [\cos\ \alpha(\cos^2\ \alpha + \sin^2\ \alpha \sin^2\ \theta)]^4$$
$$\times \left[\cos\ \alpha \cos\ \gamma + \sin\ \alpha \sin\ \gamma\left(\frac{\cos\ \theta}{\sqrt{2}} + \frac{\sin\ \theta}{2}\right)\right]^4.$$

The various angles were defined in the previous subsection. The matrix elements for such processes are

$$\langle \vec{k}, 2\vec{e}_x | \hat{T} | \vec{k}, \vec{e}_x \rangle = -2t_3 \cos\frac{k_x a}{2},$$

$$\langle \vec{k}, 2\vec{e}_y | \hat{T} | \vec{k}, \vec{e}_y \rangle = -2t_3 \cos\frac{k_y a}{2}, \tag{B8}$$

in other words like the general matrix elements of Eq. (B7), except with the appropriate value of the effective hopping integral.

The second special case involves hopping between second- and fourth-nn bipolarons. In this case, the overlap between the corresponding polarization clouds leads to

$$\frac{t_4}{t} = \langle i, i + \vec{e}_x + \vec{e}_y | i, i + \vec{e}_x + 2\vec{e}_y \rangle$$
$$= \cos^6\ \alpha[\cos^2\ \alpha + \sin^2\ \alpha \cos^2\ \theta]^4$$
$$\times [\cos\ \alpha \cos\ \beta + \sin\ \alpha \sin\ \beta \cos\ \theta]^2 \tag{B9}$$

and the matrix elements

$$\langle \vec{k}, 2\vec{e}_x \pm \vec{e}_y | \hat{T} | \vec{k}, \vec{e}_x \pm \vec{e}_y \rangle = -2t_4 \cos\frac{k_x a}{2},$$

$$\langle \vec{k}, \vec{e}_x \pm 2\vec{e}_y | \hat{T} | \vec{k}, \vec{e}_x \pm \vec{e}_y \rangle = -2t_4 \cos\frac{k_y a}{2}. \tag{B10}$$

The third special case involves hopping between second- and first nearest-neighbor bipolarons. This leads to a renormalized hopping

$$\frac{t_2}{t} = \langle i, i+\vec{e}_x | i, i+\vec{e}_x+\vec{e}_y\rangle$$
$$= \cos^6\alpha \times [\cos^2\alpha + \sin^2\alpha\cos^2\theta]^2$$
$$\times\left[\cos\beta\cos\gamma + \frac{\sin\beta\sin\gamma}{\sqrt{2}}\right]^2$$
$$\times\left[\cos\alpha\cos\gamma + \sin\alpha\sin\gamma\left(\frac{\cos\theta}{\sqrt{2}}+\frac{\sin\theta}{2}\right)\right]^2$$

and the matrix elements

$$\langle \vec{k}, \vec{e}_x \pm \vec{e}_y | \hat{T} | \vec{k}, \vec{e}_y\rangle = -2t_2\cos\frac{k_x a}{2},$$

$$\langle \vec{k}, \vec{e}_x \pm \vec{e}_y | \hat{T} | \vec{k}, \vec{e}_x\rangle = -2t_2\cos\frac{k_y a}{2}. \quad \text{(B11)}$$

Finally, for the hopping between on-site and nearest-neighbor bipolaron, the effective hopping is found to be

$$\frac{t_1}{t} = \langle i, i | i, i+\vec{e}_x\rangle$$
$$= \cos^4\alpha\cos^4(\alpha-\delta)$$
$$\times\left[\cos\delta\cos\gamma + \sin\delta\sin\gamma\left(\frac{\cos\theta}{\sqrt{2}}+\frac{\sin\theta}{2}\right)\right]^4,$$

and the matrix elements are

$$\langle \vec{k}, \vec{e}_x | \hat{T} | \vec{k}, 0\rangle = -2\sqrt{2}t_1\cos\frac{k_x a}{2},$$

$$\langle \vec{k}, \vec{e}_y | \hat{T} | \vec{k}, 0\rangle = -2\sqrt{2}t_1\cos\frac{k_y a}{2}. \quad \text{(B12)}$$

The extra factor of $\sqrt{2}$ is because of the on-site singlet normalization. Of course, for triplet states $t_1=0$ since there is no on-site triplet.

In Fig. 13(a) we plot the values of t_1/t, t_2/t, t_3/t and t_4/t vs. Ω for $\alpha_P=10$ Å^3. These should be compared with $t_{\rm eff}/t$ shown in Fig. 6. The overall changes are relatively small.

The situation for second-nearest-neighbor hopping is similar. If $\vec{\delta}$ is large enough, then the cloud overlap is the same as for individual polarons and the renormalized hopping is $t'_{\rm eff}$, giving the matrix elements

$$\langle \vec{k}, \vec{\delta}+\vec{e}_x \pm \vec{e}_y | \hat{T}' | \vec{k}, \vec{\delta}\rangle = -2t'_{\rm eff}\cos\frac{(k_x \pm k_y)a}{2}. \quad \text{(B13)}$$

Again, special care must be used for values of $\vec{\delta}$ near the edges of its area of allowed values so that the periodic boundary conditions are properly accounted for. This is done in a manner totally analogous to that explained for nearest-neighbor hopping.

There are again four special cases of different renormalization of t'. One involves the hopping between the two possible nearest-neighbor bipolaron states, which has the matrix element

$$\langle \vec{k}, \vec{e}_x | \hat{T}' | \vec{k}, \vec{e}_y\rangle = -2t'_2\left[\cos\frac{(k_x+k_y)a}{2} + \cos\frac{(k_x-k_y)a}{2}\right],$$

where

$$t'_2/t' = \langle i, i+x | i, i+y\rangle$$
$$= \left[\cos^2\gamma + \frac{1}{2}\sin^2\gamma\right]^2 \times \cos^8\alpha\left[\cos\alpha\cos\gamma + \sin\alpha\sin\gamma\left(\frac{\cos\theta}{\sqrt{2}}+\frac{\sin\theta}{2}\right)\right]^4.$$

The second involves the hopping between second- and third-nn bipolarons, as well as hopping away from a second-nn bipolaron, with the matrix elements

$$\langle \vec{k}, 2\vec{e}_x \pm 2\vec{e}_y | \hat{T}' | \vec{k}, \vec{e}_x \pm \vec{e}_y\rangle = -2t'_3\cos\frac{(k_x \pm k_y)a}{2},$$

$$\langle \vec{k}, 2\vec{e}_x | \hat{T}' | \vec{k}, \vec{e}_x \pm \vec{e}_y\rangle = -2t'_3\cos\frac{(k_x \mp k_y)a}{2},$$

$$\langle \vec{k}, 2\vec{e}_y | \hat{T}' | \vec{k}, \vec{e}_x \pm \vec{e}_y\rangle = -2t'_3\cos\frac{(k_x \mp k_y)a}{2},$$

where $t'_3 = t'\langle i, i+x+y | i, i+2x+2y\rangle = t'\langle i+x+y | i+2x\rangle$ is found to be

$$t'_3 = t'[\cos\alpha]^{10}[\cos\alpha\cos\beta + \sin\alpha\sin\beta\cos\theta]^2$$
$$\times[\cos^2\alpha + + \sin^2\alpha\cos(2\theta)]^2.$$

The third case involves hopping between first- and fourth-nn bipolarons, with matrix elements

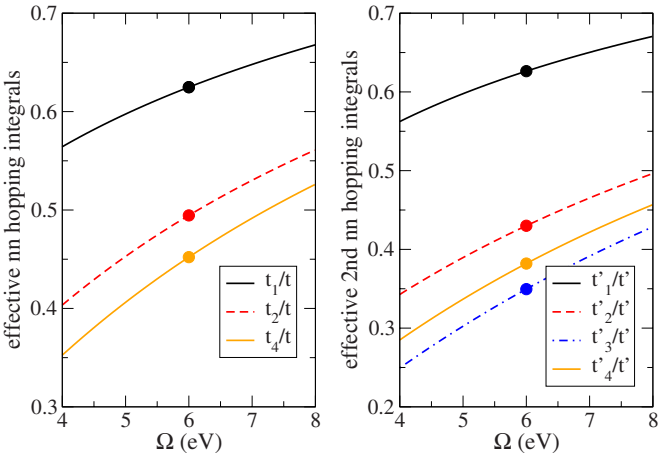

FIG. 13. (Color online) Effective hoppings for closely spaced bipolarons. For these parameters, the t_2 and t_3 curves are essentially superimposed, therefore we only show t_2/t.

$$\langle \vec{k}, 2\vec{e}_x \pm \vec{e}_y | \hat{T}' | \vec{k}, \vec{e}_x \rangle = -2t_4' \cos\frac{(k_x \pm k_y)a}{2},$$

$$\langle \vec{k}, \vec{e}_x \pm 2\vec{e}_y | \hat{T}' | \vec{k}, \vec{e}_y \rangle = -2t_4' \cos\frac{(k_x \pm k_y)a}{2},$$

where $t_4' = t' \langle i+x | i+2x+y \rangle$ equals

$$t_4' = t'[\cos\alpha]^8[\cos^2\alpha + \sin^2\alpha\cos(2\theta)]^2 \times \left[\cos\alpha\cos\gamma + \sin\alpha\sin\gamma\left(\frac{\cos\theta}{\sqrt{2}} + \frac{\sin\theta}{2}\right)\right]^4.$$

Finally, the hopping between an on-site and a second-nearest-neighbor bipolaron (possible only for singlet states) leads to

$$\langle \vec{k}, \vec{e}_x \pm \vec{e}_y | \hat{T}' | \vec{k}, 0 \rangle = -2\sqrt{2}t_1' \cos\frac{(k_x \pm k_y)a}{2},$$

where

$$t_1' = t' \langle i, i | i, i+x+y \rangle = t'[\cos\alpha\cos(\alpha-\delta)]^6[\cos(\beta-\delta)]^2.$$

The renormalized values t_1', t_2', t_3', and t_4' are shown, in units of t', in Fig. 13(b).

APPENDIX C: ESTIMATES FOR THE ACCURACY OF VARIOUS APPROXIMATIONS

In the previous sections we argued that first-order perturbation theory is reasonably accurate for our Hamiltonian, given the values of the various parameters relevant for the Fe-based superconductors. However, the Hamiltonian itself already embodies two approximations, namely (i) that only As atoms nn to a doping charge become polarized, and (ii) that dipole-dipole interactions between the various polarized As atoms are ignored. We provide here estimates for the accuracy of these approximations. We begin by discussing the single polaron.

Assume that interactions with the eight As atoms which are second nn to a charge are also included. This supplementary interaction would be described by a Hamiltonian similar to $\mathcal{H}_{\text{int}}$ of Eq. (4), except it would have a new energy scale g' and new angles describing the orientations of these Fe-As bonds.

From the definition of the interaction energy, Eq. (A4), we have

$$\frac{g'}{g} = \frac{R^2}{R'^2},$$

where $R' = \sqrt{11}a/2$ is the distance from an Fe to a second-nn As atom. This comes about because the only difference is in the electric fields created at the two sites, and these are inversely proportional to the square of the distances.

It then follows immediately that the contribution to the static polaron energy of these eight clouds would be

$$E_{\text{corr}} = 8(\Omega - \sqrt{\Omega^2 + 4g'^2}), \tag{C1}$$

which for our typical parameters is $E_{\text{corr}} = -1.2$ eV. Of course, considering the polarization of even more distant As atoms would lower this energy even more.

However, this decrease is more than compensated for by consideration of dipole-dipole interactions. To estimate these energies, let us consider only the six pair interactions between the four largest dipole moments on the nn As sites. Consider a pair of two such dipoles, with moments $\vec{p}_1$ and $\vec{p}_2$. Their magnitude is given by Eq. (A10) and their orientations are straightforward to determine, as is the distance $\vec{d}$ between them. Using these values, we find for any such pair that

$$E_{\text{d-d}} = \frac{\vec{p}_1 \cdot \vec{p}_2}{d^3} - 3\frac{(\vec{p}_1 \cdot \vec{d})(\vec{p}_2 \cdot \vec{d})}{d^5} = \frac{10\alpha_p\Omega}{3\sqrt{2}a^3}\frac{g^2}{\Omega^2 + 4g^2}.$$

For our typical parameters, $E_{\text{d-d}} = 0.66$ eV and therefore the total for the six pair interactions is ≈ 4 eV. Inclusion of contributions from interactions with the dipoles on the second nn As atoms will decrease this because nn and second-nn dipoles closest to each other are now roughly parallel, not antiparallel, to each other.

Taken together and without further corrections, these two energies would renormalize $E_{P,GS}$ to about half the value predicted in their absence. If we keep adding further rows of neighbors into the calculation, the polaron energy saturates (slowly) to around -1.6 eV (of course, one expects the long-range dependence of the electric field to be screened away from a $1/R^2$ dependence. The precise result will depend on how this screening occurs). Having extended clouds would also lower the effective hoppings somewhat more, although we expect this to be a much smaller effect: clouds which are far from the electronic charge are not changed much if the charge moves by one site. As a result, their contribution to the total overlap should be very close to 1.

Although the renormalization of the static part of the polaron energy is quite substantial, these corrections do not have nearly as large an effect on the bipolaron interaction energies U_0, U_1, and U_2. The reason is that these are differences between the true bipolaron energy and the energy of two free polarons, and therefore many contributions from both the extended clouds and the dipole-dipole interactions cancel each other out.

For example, consider the effects of these corrections on U_1, which is the most interesting energy. For two polarons at an infinite distance from each other, the dipole-dipole correction is 12 $E_{\text{d-d}}$ and there are a total of 16 second-nn extra clouds. For a nn bipolaron, the dipole-dipole energy is roughly 11 $E_{\text{d-d}}$ because the two As tetrahedra share one side (of course, the two central As atoms have somewhat different dipole moments pointing in somewhat different directions, and also there are smaller contributions from interactions between the noncentral As atoms belonging to different Fe, but 11 $E_{\text{d-d}}$ should be a reasonable guess). This configuration would only have 12 second-nn extra clouds. Subtracting these corrections leads to an overall correction of U_1 roughly equal to $-\frac{1}{2}E_{\text{corr}} - E_{\text{d-d}} \approx 0$. In reality, the energy is lowered because the close location of the two charges implies larger electric fields at all sites for the nn bipolaron, therefore larger clouds. We find that as we increase the number of As neighbors included in the cloud, U_1 is lowered from ≈ -1 eV

(the value we find when the approximations are made) to −2.87 eV if we include second-nn and dipole-dipole interactions, to −4 eV if more and more neighbors are added. Again, one expects that the electric fields will be screened over some finite distance which will decide the precise value. The point, though, is that relaxing the approximations increases this attraction energy, in other words the physics we discuss here becomes more relevant, not less so.

[1] P. W. Anderson, Science **177**, 393 (1972).
[2] J. Bardeen, L. N. Cooper, and J. R. Schrieffer, Phys. Rev. **106**, 162 (1957).
[3] J. G. Bednorz and K. A. Müller, Z. Phys. B: Condens. Matter **64**, 189 (1986).
[4] Y. Kamihara, H. Hiramatsu, M. Hirano, R. Kawamura, H. Yanagi, T. Kamiya, and H. Hosono, J. Am. Chem. Soc. **128**, 10012 (2006).
[5] Y. Kamihara, T. Watanabe, M. Hirano, and H. Hosono, J. Am. Chem. Soc. **130**, 3296 (2008).
[6] H. Takahashi, K. Igawa, K. Arii, Y. Kamihara, M. Hirano, and H. Hosono, Nature (London) **453**, 376 (2008).
[7] X. H. Chen, T. Wu, G. Wu, R. H. Liu, H. Chen, and D. F. Fang, Nature (London) **453**, 761 (2008).
[8] G. F. Chen, Z. Li, D. Wu, G. Li, W. Z. Hu, J. Dong, P. Zheng, J. L. Luo, and N. L. Wang, Phys. Rev. Lett. **100**, 247002 (2008).
[9] G. A. Sawatzky, I. S. Elfimov, J. van den Brink, and J. Zaanen, EPL **86**, 17006 (2009).
[10] F. C. Zhang and T. M. Rice, Phys. Rev. B **37**, 3759 (1988).
[11] C. Cao, P. J. Hirschfeld, and H. P. Cheng, Phys. Rev. B **77**, 220506(R) (2008).
[12] K. Haule, J. H. Shim, and G. Kotliar, Phys. Rev. Lett. **100**, 226402 (2008).
[13] Z. P. Yin, S. Lebègue, M. J. Han, B. P. Neal, S. Y. Savrasov, and W. E. Pickett, Phys. Rev. Lett. **101**, 047001 (2008).
[14] Q. Si and E. Abrahams, Phys. Rev. Lett. **101**, 076401 (2008).
[15] C. Xu, M. Müller, and S. Sachdev, Phys. Rev. B **78**, 020501(R) (2008).
[16] W.-Q. Chen, K.-Y. Yang, Y. Zhou, and F.-C. Zhang, Phys. Rev. Lett. **102**, 047006 (2009).
[17] T. A. Maier, and D. J. Scalapino, Phys. Rev. B **78**, 020514(R) (2008).
[18] S. Raghu, Xiao-Liang Qi, Chao-Xing Liu, D. J. Scalapino, and Shou-Cheng Zhang, Phys. Rev. B **77**, 220503(R) (2008).
[19] P. A. Lee and X.-G. Wen, Phys. Rev. B **78**, 144517 (2008).
[20] D. J. Singh and M.-H. Du, Phys. Rev. Lett. **100**, 237003 (2008).
[21] A. S. Alexandrov and N. F. Mott, *Polarons and Bipolarons* (World Scientific, Singapore, 1995), and references therein.
[22] W. A. Little, Phys. Rev. **134**, A1416 (1964).
[23] D. Allender, J. Bray, and J. Bardeen, Phys. Rev. B **7**, 1020 (1973).
[24] J. E. Hirsch and F. Marsiglio, Phys. Rev. B **39**, 11515 (1989); Physica C **162-164**, 591 (1989).
[25] J. E. Hirsch and S. Tang, Solid State Commun. **69**, 987 (1989).
[26] F. Marsiglio and J. E. Hirsch, Physica C **468**, 1047 (2008).
[27] G. L. Goodvin, M. Berciu, and G. A. Sawatzky, Phys. Rev. B **74**, 245104 (2006).
[28] D. K. G. de Boer, C. Haas, and G. A. Sawatzky, Phys. Rev. B **29**, 4401 (1984).
[29] D. H. Lu, M. Yi, S.-K. Mo, A. S. Erickson, J. Analytis, J.-H. Chu, D. J. Singh, Z. Hussain, T. H. Geballe, I. R. Fisher, and Z.-X. Shen, Nature (London) **455**, 81 (2008).
[30] R. Klingeler, N. Leps, I. Hellmann, A. Popa, C. Hess, A. Kondrat, J. Hamann-Borrero, G. Behr, V. Kataev, and B. Buechner, arXiv:0808.0708 (unpublished).
[31] H.-J. Grafe, D. Paar, G. Lang, N. J. Curro, G. Behr, J. Werner, J. Hamann-Borrero, C. Hess, N. Leps, R. Klingeler, and B. Büchner, Phys. Rev. Lett. **101**, 047003 (2008).
[32] A. Macridin, G. A. Sawatzky, and Mark Jarrell, Phys. Rev. B **69**, 245111 (2004).